

DEFINITION OF A CONTROL SCHEME FOR A COORDINATED MANAGEMENT OF LARGE OFFSHORE WIND FARMS CONNECTED VIA HVDC LINKS

F. Careri, C. Genesi, P. Marannino, M. Montagna, P. Raboni, S. Rossi, I. Siviero
Department of Electric Engineering, University of Pavia
Pavia, Italy
francesco.careri@unipv.it

Abstract – This paper proposes the development of an appropriate control system for the real-time management of large offshore Doubly-Fed Induction Generator (DFIG) based wind farms, connected to the transmission network by Voltage Source Converter High Voltage Direct Current (VSC-HVDC) link. In this plant layout, variable frequency operation lets wind turbines to work on a wider range of wind speed values, limiting the generator slip and improving at the same time the energy production. The VSC-HVDC sending end converter and the DFIGs grid side and rotor side converters are modelled as ideal three-phase voltage generators: the values of some control variables are calculated by a two-step optimization procedure coded in MATLAB® programming language: a central optimizer, which maximizes the overall power production of the whole wind farm and a local optimizer, which gives the appropriate set-point signals for each wind turbine. The aforementioned configuration and the control solutions applied to each wind turbine have been modelled in Simulink® environment. Tests are carried out on a wind farm with 50 wind turbines.

Keywords: offshore wind farms, DFIG, VSC-HVDC link, variable frequency operation, online optimization algorithm.

1 INTRODUCTION

Despite the global financial crisis, in recent years wind industry has experienced a continuous growth at a very rapid rate. Nowadays, wind production represents one of the most attractive options among renewable energy sources (RES) in order to satisfy the increasing global energy demand thanks to its virtual availability throughout the world, its low environmental impact and its competitiveness with new-built conventional generation technologies. Furthermore, wind industry may create thousands of quality jobs in the manufacturing sector. In 2009, more than 38 GW of new wind power capacity was installed, bringing the total installed capacity up to 158.5 GW around the world, with an increase of 31.7% compared to the previous year [1].

Although the great theoretical availability of wind energy, the intensive exploitation has led to a progressive saturation of the best sites for the installation of onshore wind farms. This is an issue which has become relevant in those countries where wind power penetration is already high, e.g. in European countries. There-

fore, an increasing interest is addressed to offshore applications, which can ensure a larger availability of sites, a better wind resource and a strong reduction of visual impact. With regard to EU countries, which are pioneers in offshore wind applications, the economically competitive offshore potential exploitable by 2020 is 2600 TWh, equal to the 60-70% of the expected electricity demand [2].

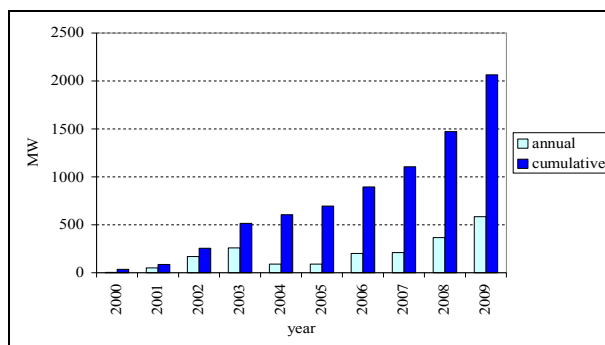


Figure 1: Annual and cumulative installed EU offshore wind capacity (2000-2009).

Figure 1 shows the annual and cumulative capacity trends for European offshore installations in last decade: with over 2 GW of power installed by the end of 2009, offshore wind farms accounted for 2.8% of installed EU wind power capacity and, with 592 MW, for 5.8% of annual capacity [3], [4]. In 2009, the European Wind Energy Association (EWEA) proposed the challenging but manageable target of 40 GW of offshore wind power capacity in 2020 [5]. To exploit this potential, an increasing number of new wind farms will be located far away from the coast, more than 100 km, where the wind characteristics are better. This kind of installations usually exploits DFIGs, requiring a back-to-back converter, coupled with pitch controlled blade turbine, in order to allow a variable speed operation [6].

Notwithstanding, to deliver real power flows to the land over such long distances, HVAC (High-Voltage Alternating Current) transmission has many disadvantages, due to high charging currents, both from the technical and economic point of view. Therefore, the high reactive power associated to underwater cables suggests the use of HVDC transmission. The increasing rating and improved performance of self-commutated

semiconductor devices has made possible the diffusion of VSC-HVDC transmission, which offers the following primary advantages with respect to conventional line commutated conversion based on current source converters [7]:

- each end of the link can be controlled to absorb/generate reactive power independently of the real power transfer,
- the DC link can be connected to a weak, and even passive, AC network,
- VSC transmission can be designed to provide a variety of ancillary services to the interconnected AC systems (reactive power compensation, harmonic and unbalanced voltage compensation, flicker elimination, etc).

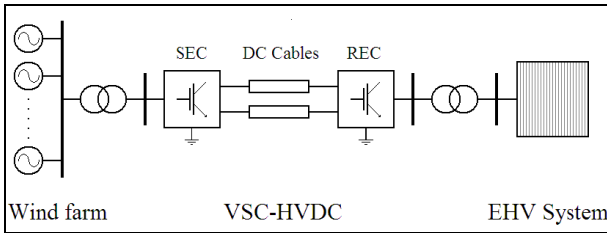


Figure 2: Coordination between DFIG based wind farm and VSC-HVDC link

Therefore, it appears to be useful to investigate the synergy of these well-known technologies, as shown in Figure 2. In addition to the aforementioned benefits, this power plant layout allows variable frequency operation, to extend the mechanical speed range of wind turbines. In [8] this operating condition is described with the aim of avoiding a more expensive sizing of the converter. The paper primarily focuses on the speed variability expansion of the wind turbines for optimizing the power production of the whole wind farm avoiding the adoption of an higher rated back-to-back DFIG converter: assuming the AC network frequency as a further degree of freedom, it could enhance the plant efficiency.

The aim of this paper is to develop an appropriate coordinated control system which could allow an optimal exploitation of the variable wind resource, taking into due account the dynamic behaviour of both DFIGs and VSC-HVDC link. A modified version of an online optimization procedure [11], which defines the appropriate set-point signals for the proposed control system, is described in Section 2. In Section 3 the proposed control system, developed in the Simulink® environment, and its regulation loops are shown. In order to prove its goodness, simulations are carried out on a wind farm composed by 50 wind turbines. Results, described in Section 4, show the model validation, highlighting how the proposed tool is suitable for an optimized and coordinated real time management of large offshore wind farms.

2 ONLINE OPTIMIZATION PROCEDURE

This section summarizes the features of the proposed two-step optimization procedure and some implementation issues deriving from its online application to supply the reference signals of DFIGs and VSC-HVDC control schemes.

2.1 Central Optimizer (CO) Mathematical Model

The optimization designed for the CO pursuits the maximization of the total wind power plant production. The variables are the offshore grid frequency, the generators' slips and the pitch angles. The function is parameterized by means of the wind speed for each turbine.

The mathematical model is as follows:

$$\max_{f, s_i, \beta_i} \sum_{i=1}^{N_T} P_{m_i} (f, s_i, v_{wind_i}, \beta_i) \quad (1)$$

subject to:

$$f_{\min} \leq f \leq f_{\max} \quad (2)$$

$$\beta_{\min} \leq \beta_i \leq \beta_{\max} \quad \forall i \in N_T \quad (3)$$

$$\omega_{r_{\min}} \leq \omega_i \leq \omega_{r_{\max}} \quad \forall i \in N_T \quad (4)$$

$$\frac{1}{1-s_i} P_{m_i} (f, s_i, v_{wind_i}, \beta_i) \leq K_{ps} P_{sn} \quad \forall i \in N_T \quad (5)$$

$$-P_{rn} \leq \frac{-s_i}{1-s_i} P_{m_i} (f, s_i, v_{wind_i}, \beta_i) \leq P_{rn} \quad \forall i \in N_T \quad (6)$$

$$T_{m_i} (f, s_i, v_{wind_i}, \beta_i) \leq T_n \quad \forall i \in N_T \quad (7)$$

where s_i , β_i , ω_i , P_{m_i} and T_{m_i} are the generator slip, the pitch angle, the mechanical rotational speed, the power production and the mechanical torque respectively, while v_{wind_i} is the measured (or predicted) wind speed for each turbine. Input v_{wind_i} may be different from one turbine to another due to aerodynamic array effect [9].

In (1) the power production (neglecting both mechanical and electrical losses) is a function of the generator slip, the pitch angle, the stator frequency and the wind speed:

$$P_{m_i} = c_{p_i} (\lambda_i, \beta_i) \frac{\rho A}{2} v_{wind_i}^3 \quad \forall i \in N_T \quad (8)$$

where $c_{p_i} (\lambda_i, \beta_i)$ [10] is the power coefficient and

$$\lambda_i = \frac{\omega_i R}{v_{wind_i}}$$

is the tip-speed ratio (R is the turbine radius). The rotational speed is provided by:

$$\omega_i = \frac{2\pi}{pp} f (1-s_i) \quad \forall i \in N_T \quad (9)$$

pp being the number of pole pairs.

The problem constraints are the upper and lower bounds on offshore grid frequency (2), pitch angle (3), rotational speed (4) and rotor active power flow (6).

Furthermore, the stator active power flow (5) of each generator as well as the mechanical torque (7) must respect its maximum limits. The rotor active power flow may be positive or negative depending on the slip sign (positive or negative for under-synchronous or super-synchronous operation). Stator power flow limit is calculated with respect to its rated value by means of the overload coefficient K_{ps} (5). Rotor overload is not allowed in order to adopt a down-rated DFIG back-to-back converter. The variation of the offshore grid frequency must reflect an equal offshore voltage change to prevent the stator flux decreasing [14]. Constraint (2) considers the limits in variation of both frequency and voltage of VSC-HVDC link and the insulation limits of the devices in the offshore wind farm. Constraint (4) considers the mechanical limits of the turbine working under a fixed rotational speed range. Since equation (9) shows the relationship among mechanical rotational speed, generator slip and offshore grid frequency (equal to stator frequency), upper and lower bound constraints (4) affects both slip and frequency. In steady state conditions, the electromechanical torque is equal to the mechanical one. From [13], in stator voltage synchronous reference frame, the electromechanical torque is:

$$T_{em} = 3pp \operatorname{Im} \left[\bar{\phi}_s \cdot \bar{I}_r^* \right] \approx 3pp\phi_s i_{rd} \quad (10)$$

Then, if the stator flux ϕ_s is constant, the electromechanical torque will be proportional to the d component of the rotor current (i_{rd}). Considering the DFIG mathematical model, the q component of the rotor current is the driver for the reactive power (generated from DFIG) changing. In this paper it is assumed that reactive power balance in the wind farm grid is mainly supported by the VSC-HVDC Sending End Converter (SEC) [8]: the DFIG wind turbines are operated close to unity power factor. Therefore, the rotor current magnitude is mainly determined by i_{rd} . Considering (9), the upper bound constraint (7) is essentially a limitation on rotor current. Therefore, as well as for (6), it is set equal to rated torque, in order to avoid rotor converter damages. Enforcing (4) and (7) together in the model, it is possible to bound the maximum mechanical power. The stator and rotor power flows can be written in terms of stator and rotor voltages (\bar{V}_s and \bar{V}_r) and currents (\bar{I}_s and \bar{I}_r):

$$\Re \left\{ 3 \cdot \bar{V}_s \cdot \bar{I}_s^* \right\} = \frac{1}{1-s} P_m \quad (11)$$

$$\Re \left\{ 3 \cdot \bar{V}_r \cdot \bar{I}_r^* \right\} = \frac{-s}{1-s} P_m \quad (12)$$

The right hand side of equations (11) and (12) are limited by constraints (5) and (6), while the stator frequency as well as the stator voltage are bounded by equation (2).

As will be explained in Section 3, given the stator, the rotor and the Grid Side Converter (GSC) voltage equations in steady state condition, considering the equality

of the real power flow across DFIG Rotor Side Converter (RSC) and GSC, and that the generators work close to unity power factor (13):

$$\left| 3 \cdot \bar{V}_s \cdot \bar{I}_s^* + 3 \cdot \bar{V}_{gsc} \cdot \bar{I}_{gsc}^* \right| = P_m \quad (13)$$

all electric controlled variables ($\bar{V}_s, \bar{I}_s, \bar{V}_{gsc}, \bar{I}_{gsc}, \bar{V}_r$ and \bar{I}_r) are bounded.

2.2 Implementation issues

The variables corresponding to the model solution (1)-(7) could result in unfeasible fast changes especially for offshore grid frequency and mechanical rotational speed. This could lead to huge kinetic energy variations in a very small time and frequency transients dangerous for system stability. To avoid these kind of problems, the upper and lower limits of the constraints (2) and (4) are suitably set, on the basis of the previous values of ω and f , to allow variations under a fixed threshold. This is equivalent to impose upper and lower bounds on $\Delta f / \Delta T$ and $\Delta \omega / \Delta T$, fixed a suitable ΔT .

The model (1)-(7) is a non linear optimization problem with real variables: to solve it, an Interior Point (IP) technique included in the MATLAB® Optimization Toolbox™ (function *fmincon*) was applied. To reduce the computational time, the Hessian matrix of the Lagrangian function, the gradient of the objective function and the Jacobian matrix of the constraints were analytically determined. In any case, the computational time reaches 0.5 s when the number of turbines is high (50 for instance). In this work a wind speed prediction technique has been developed, in order to consider the delay due to computational, communication and actuators time. A non linear least-squares formulation has been used to fit a nonlinear model to the previous five wind speed samples: for each sample, the predicted value is the mean of the wind speed in the selected time interval (for instance one second). However the predicted wind speed may be slightly different from its actual value. Then, to fulfill constraints (5) - (7) for each turbine considering the actual wind speed, another optimization procedure called Local Optimizer (LO) has been designed. LO uses the same mathematical model of CO, but it fixes the frequency at the value calculated from CO. LO maximizes the power produced by a single turbine modifying the pertinent variables. The resulting problem so built is very fast to solve because manages only two variables. Therefore, for each run of CO, the LO can be solved several times: in this way LO modifies in real time the pitch angle and the slip of each turbine on the basis of the measured wind speed (Figure 3). The resulting offshore grid frequency (calculated by CO) and generators' rotational speeds (evaluated by LO) are sent to VSC-HVDC Sending End Converter (SEC) and DFIG RSC control schemes respectively. Instead the pitch angles calculated by LO are directly supplied to turbines' pitch actuators, in order to perform active stall control.

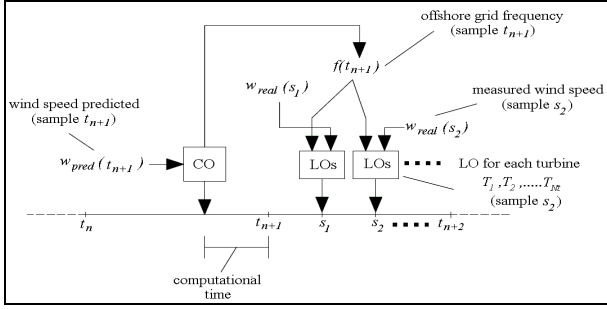


Figure 3: Time line of the online procedure

3 COORDINATED CONTROL SCHEME OF VSC-HVDC SEC AND DFIG BASED WIND FARM

3.1 VSC-HVDC SEC model

The mostly used and simple VSC-HVDC system is based on a two-level configuration. The topologically identical receiving end converter (REC) and the sending end converter (SEC) are controlled independently.

For this paper, a complete VSC-HVDC modelling is not performed: however, in order to allow a variable frequency operation, the wind farm side windings of the transformer connected to the SEC have been modelled at first as an ideal three-phase voltage generator.

Thanks to this assumption, it is imposed the variation of the voltage magnitudes at the DFIGs stator windings in agreement with the offshore grid frequency, according to the optimum point found by means of the optimization procedure described in Section 2: therefore, both voltages and frequency of the offshore AC network are imposed without control loops structure, in order to maintain a constant stator flux at the DFIGs.

3.2 RSC control system

According to [12], in normal operating mode, when both rotor voltage and rotor current are controlled by means of the semiconductor switches, the RSC regulation loop allows the independent control of both real and reactive power flows of the machine.

Assuming a steady-state condition and neglecting the stator resistive voltage drop, in a stator voltage oriented reference frame ($\bar{V}_s = v_s^d$), rotating at synchronous speed ($\omega_s = 2\pi f$), the stator voltage and the stator flux are given by:

$$\bar{V}_s = j\omega_s \bar{\phi}_s \quad (14)$$

$$\bar{\phi}_s = (L_s + M)\bar{I}_s + M\bar{I}_r = L_s\bar{I}_s + M\bar{I}_r \quad (15)$$

where L_s and M are stator and mutual inductance, while \bar{I}_s , \bar{I}_r are stator and rotor current.

Combining (14) and (15) and applying the Park transformation, the d-q rotor current components are evaluated by:

$$\begin{cases} i_r^d = -\frac{L_s}{M} i_s^d \\ i_r^q = -\frac{v_s^d}{\omega_s M} - \frac{L_s}{M} i_s^q \end{cases} \quad (16)$$

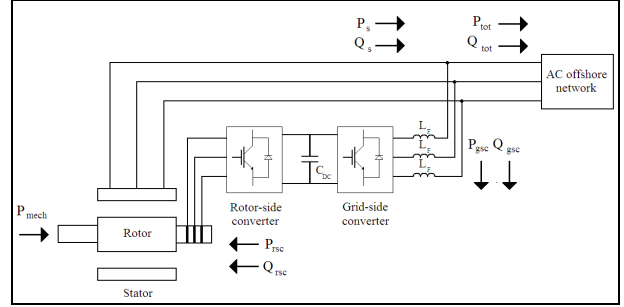


Figure 4: Power flow of an ideal DFIG [13]

Assuming both real and reactive stator power reference values, as shown in (17), neglecting all power losses and taking into account the DFIG power flow (Figure 4) the stator current set points are given by:

$$\bar{S}_s = \bar{V}_s \cdot \bar{I}_s^* \Rightarrow \begin{cases} p_{s,ref} = v_s^d i_s^d \\ q_{s,ref} = -v_s^d i_s^q \end{cases} \quad (17)$$

$$\begin{cases} i_{s,ref}^d = \frac{p_{s,ref}}{v_s^d} = \frac{p_{tot} - p_{gsc}}{v_s^d} \\ i_{s,ref}^q = -\frac{q_{s,ref}}{v_s^d} = -\frac{q_{tot} - q_{gsc}}{v_s^d} \end{cases} \quad (18)$$

where p_{tot} and p_{gsc} have the meaning shown in Figure 4.

Therefore, from (16) and (18), the rotor current can be evaluated by:

$$\begin{cases} i_r^d = -\frac{L_s}{M} \frac{p_{tot} - p_{gsc}}{v_s^d} \\ i_r^q = -\frac{v_s^d}{\omega_s M} + \frac{L_s}{M} \frac{q_{tot} - q_{gsc}}{v_s^d} \end{cases} \quad (19)$$

In the aforementioned hypothesis, the rotor voltage and the rotor flux equations are given by:

$$\bar{V}_r = R_r \bar{I}_r + j(\omega_s - \omega_r) \bar{\phi}_r \quad (20)$$

$$\bar{\phi}_r = (l_r + M)\bar{I}_r + M\bar{I}_s = L_r \bar{I}_r + M\bar{I}_s \quad (21)$$

where R_r , L_r are rotor resistance and inductance and $\omega_r = 2\pi \cdot f \cdot (1-s)$.

Matching (20) and (21), introducing the leakage factor $\sigma = \left(1 - \frac{M^2}{L_s L_r}\right)$, through algebraic manipulation, the rotor voltage can be rewritten as:

$$\bar{V}_r = \bar{I}_r (R_r + js\sigma L_r \omega_s) + \frac{sM}{L_s} \bar{V}_s \quad (22)$$

and in d-q coordinates in:

$$\begin{cases} v_r^d = v_r^{d'} - s\sigma L_r \omega_s i_r^q + \frac{sM}{L_s} v_s^d \\ v_r^q = v_r^{q'} + s\sigma L_r \omega_s i_r^d \end{cases} \quad (23)$$

Looking at (23), the RSC control system is non linear and coupled. The voltage drops across the rotor resistance $R_r \bar{I}_r$ in the d-q domain are the outputs of a current control: adopting PI controllers, the control law in Laplace domain is given by (24). Other terms of (23) are summed after the PI control.

$$\begin{cases} v_r^{d'} = R_r i_r^d(s) = \left(K_{P,rsc} + \frac{K_{I,rsc}}{s} \right) \cdot [i_{r,ref}^d(s) - i_r^d(s)] \\ v_r^{q'} = R_r i_r^q(s) = \left(K_{P,rsc} + \frac{K_{I,rsc}}{s} \right) \cdot [i_{r,ref}^q(s) - i_r^q(s)] \end{cases} \quad (24)$$

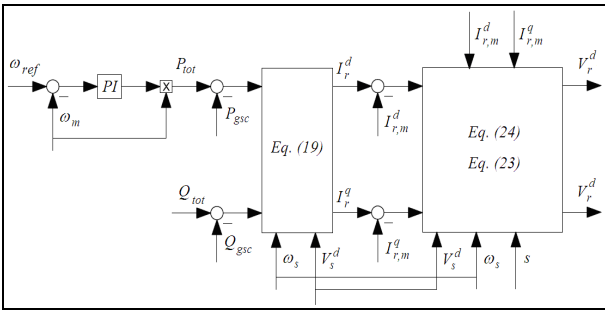


Figure 5: RSC control scheme: ω_m , $I_{r,m}^d$, $I_{r,m}^q$ (measured ω , I_r^d and I_r^q)

In Figure 5 is shown the RSC control scheme: the signals ω_{ref} is calculated by LO while p_{tot} is found by means of a PI control:

$$T(s) = \left(K_{P,speed} + \frac{K_{I,speed}}{s} \right) \cdot [\omega_{ref}(s) - \omega_m(s)] \quad (25)$$

$$P_{tot} = T \cdot \omega_m \quad (26)$$

In this paper, the reactive power reference q_{tot} is set to zero in order to allow the generator to work with unity power factor. The signals v_r^d and v_r^q are used to drive the RSC.

3.3 DC link control system

The DC link provides an asynchronous connection between the converters, decoupling the rotor side frequency from the grid side one: a capacitor is used to smooth the dc voltage variations due power imbalances. Neglecting the converter losses, the time behavior of the DC bus is given by:

$$v_{DC} = \int \frac{P_{gsc} - P_{rsc}}{C v_{DC}} dt + v_{DC}(0^+) \quad (27)$$

$$\begin{cases} P_{rsc} = v_{rsc}^d i_{rsc}^d + v_{rsc}^q i_{rsc}^q \\ P_{gsc} = v_{gsc}^d i_{gsc}^d + v_{gsc}^q i_{gsc}^q \end{cases} \quad (28)$$

A PI controller receives in input the DC voltage error: the output of this control is the $i_{gsc,ref}^d$ (29), which is sent to the GSC control loop.

$$i_{gsc,ref}^d(s) = \left(K_{P,DC} + \frac{K_{I,DC}}{s} \right) \cdot [v_{DC,ref}(s) - v_{DC}(s)] \quad (29)$$

3.4 Grid side converter (GSC) control system

As shown in Figure 4, AC offshore network and GSC are connected through a R-L filter, in order to smooth the converter current waveform.

A PI control loop (30), faster than the DC one, is used to enforce the GSC voltages (31):

$$\begin{cases} v_{gsc}^{d'} = \left(K_{P,gsc} + \frac{K_{I,gsc}}{s} \right) \cdot [i_{gsc,ref}^d(s) - i_{gsc}^d(s)] \\ v_{gsc}^{q'} = \left(K_{P,gsc} + \frac{K_{I,gsc}}{s} \right) \cdot [i_{gsc,ref}^q(s) - i_{gsc}^q(s)] \end{cases} \quad (30)$$

$$\begin{cases} v_{gsc}^d = v_s^d - R_F i_{gsc}^d + \omega_s L_F i_{gsc}^q - v_{gsc}^{d'} \\ v_{gsc}^q = -R_F i_{gsc}^q - \omega_s L_F i_{gsc}^d - v_{gsc}^{q'} \end{cases} \quad (31)$$

In this work, the $i_{gsc,ref}^q$ is set to a constant value close to zero. Concerning reactive current generation, the system provides an additional degree of freedom that can be used, e.g. for providing enhanced voltage support to the grid during faults. However, the analysis of this aspect is beyond the aims of this paper.

4 TESTS AND RESULTS

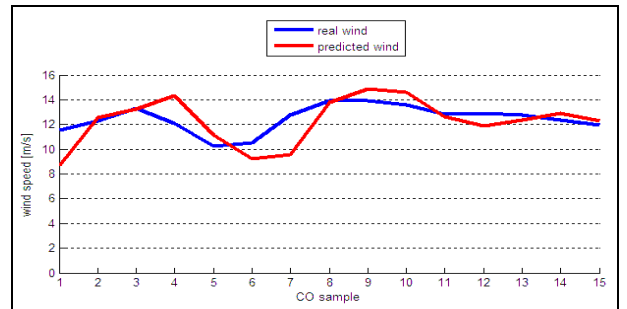


Figure 6: Trend of wind speed and its prediction

Tests are carried out in order to study the behavior of the proposed plant layout for a given wind speed profile: it is assumed a 45 seconds time interval, which corresponds to 15 CO and 450 LO samples. The adopted wind speed trend [10] and its prediction, computed by means of the methodology described in 2.2, are shown in Figure 6. In this work it is assumed to neglect all the power losses (“lossless DFIG”) and to adopt a single bus model for the AC offshore grid, in order to not consider its topology. The wind farm is composed by 50 DFIGs (five row of ten turbines): the main machine characteristics [15], are exposed in Table 1, while other electric parameters are obtained from [16]. In order to consider the mutual shading effect

between turbines, it is assumed a 2% speed decrease among machines belonging to two subsequent row [9], while turbines pertinent to the same row it is assumed to be characterized by equal wind speed.

The continuous-time dynamic model of the wind turbine, as well as the proposed control system, are developed in the Simulink® environment.

Rotor diameter	77 m
Cut-in wind speed	3.5 m/s
Cut-out wind speed	20-25 m/s
Gearbox ratio	1:104
Rated power	1.5 MW
Rated wind speed	13 m/s
Pole pairs	2
Nominal frequency	50 Hz

Table 1: Main data of the adopted DFIG turbine

4.1 Optimization procedures outputs

The proposed procedures have been tested considering the wind speed trends shown in Figure 6: CO pursues the maximization of the objective function assuming the predicted wind speed trend, while LO considers the actual wind trend.

Constraints	Upper bound	Lower bound
(2)	60 Hz	40 Hz
(3)	45°	0°
(4)	251 rad/s	84 rad/s
(5)	1.584 MW	0
(6)	177 kW	-177 kW
(7)	8.42 kNm	0
$\Delta f/\Delta T$ (CO)	0.66 Hz/s	-0.66 Hz/s
$\Delta \omega/\Delta T$ (CO, LO)	1.66 rad/s ²	-1.66 rad/s ²

Table 2: CO and LO upper and lower bounds values

The upper and lower bounds on constraint (2) are determined by the maximum voltage of the devices as well as the allowable rotor currents: not having access to suitable datasheets, it is assumed a $\pm 20\%$ frequency range (with respect to the nominal quantity), as stated in [8]. Upper and lower bound values are shown in Table 2: $\Delta f/\Delta T$ and $\Delta \omega/\Delta T$ represent the maximum variable variation between two adjacent samples, as discussed in 2.2. For the upper bound (5) it is assumed $K_{ps} = 1.2$. The limits (6) are given assuming a down-rated back-to-back converter, with a sizing lower than common DFIG applications: this choice lead to a reduction of the rotor power flow and, therefore, the converter switching losses.

Optimization results are shown in Figure 7 - Figure 11. When the wind speed assumes high values (in sam-

ples 2-4 and 8-10), the torque limit is near to its upper bound: indeed, the pertinent pitch angles increase (Figure 8).

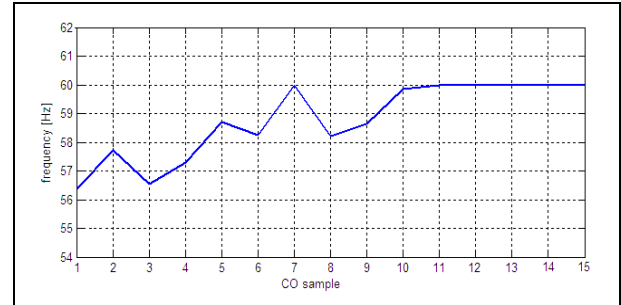


Figure 7: CO: offshore AC network frequency

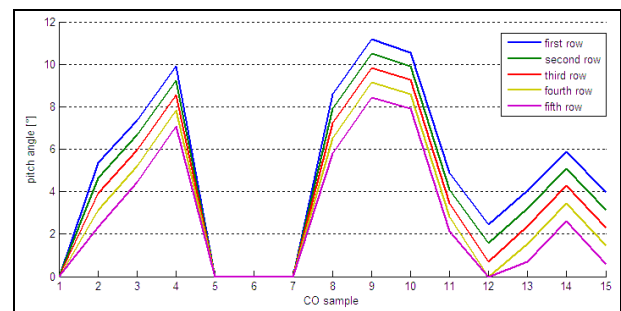


Figure 8: CO: pitch angles

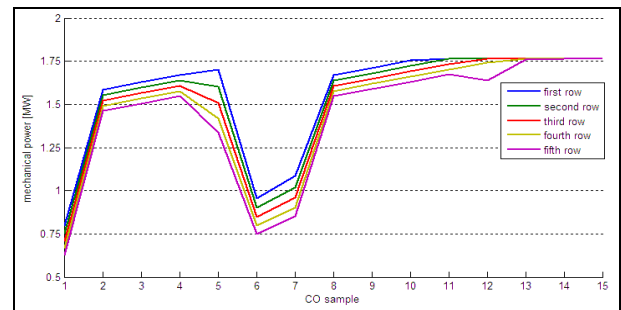


Figure 9: CO: mechanical power

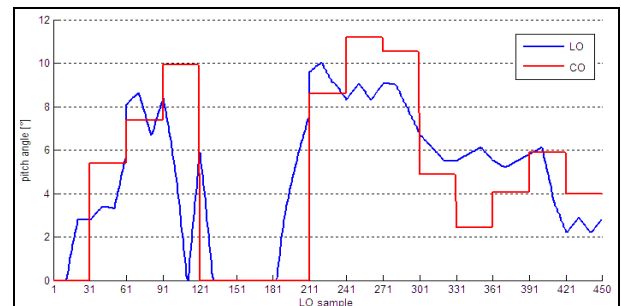


Figure 10: Comparison between CO and LO: pitch angle, first row

It can be seen the shift of the CO and LO trends due to the time delay introduced by adopting different wind

trends: the lower is this time interval, the more accurate are the set point signals given to the control system. Therefore, LO allows the DFIG to work in highly variable wind speed conditions, while maximizing its power production.

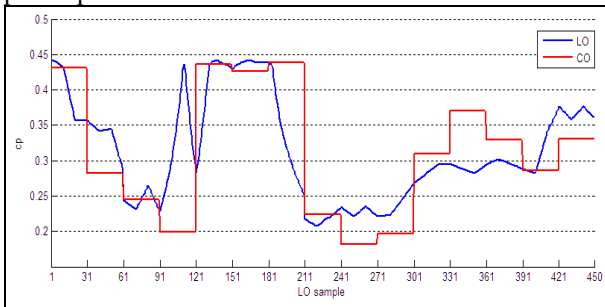


Figure 11: Comparison between CO and LO: power coefficient, first row

4.2 Simulation results

The developed time-continuous dynamic model has been tested considering the actual wind speed trend shown in Figure 6. Simulation results, pertinent to a wind turbine belonging to the first row, are exposed in Figure 12 and Figure 13. As it can be seen in the zoom of Figure 12, there is a good tracking of the DFIG mechanical speed to the set-point signal given by the LO. However, a too fast tracking can cause heavy kinetic energy variations which may lead to dangerous mechanical behaviour of the machine: this aspect proves the usefulness of enforcing the $\Delta\omega/\Delta T$ constraints.

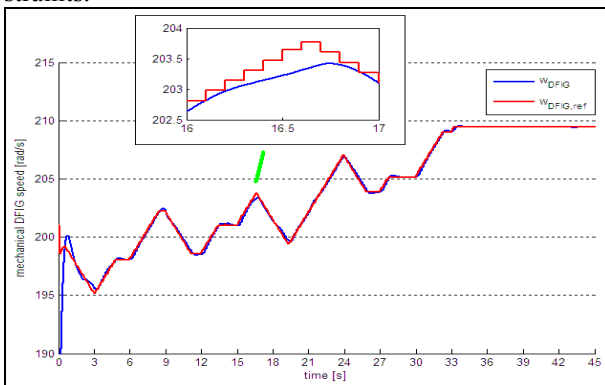


Figure 12: Mechanical DFIG speed and its set point, first row

Furthermore, the slope of the rotational speed during its variations is the same for all simulation period: this is due to the $\Delta\omega/\Delta T$ constraint. Figure 12 also shows that when the rotational speed reaches high values, its trend is homothetic to the frequency, while this it does not happen in presence of low rotational speed. Indeed when the rotor power flow is not binding (low wind speed thus low rotational speed), the mechanical speed may change for both frequency and slip variation while,

when rotor power flow reaches its maximum limits, only frequency can be increased.

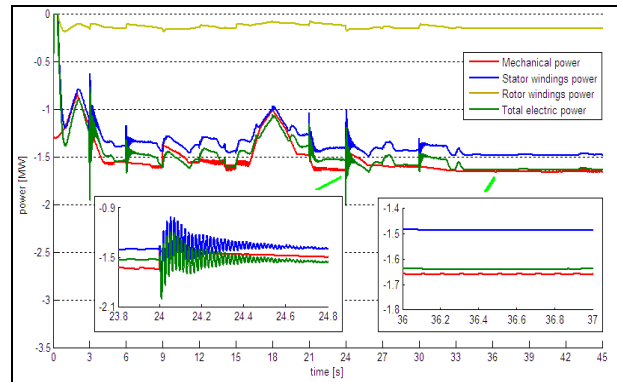


Figure 13: Mechanical, rotor, stator and electric DFIG powers, first row

4.3 Variable vs. fixed frequency operation

To prove the goodness of variable frequency operation in terms of maximizing the total electric power produced by wind farm, it has been carried out another simulation using the same procedure at fixed frequency operation. Results in terms of total electric power produced by wind farm, represented according to the generator reference direction, are shown in Figure 14.

Considering the adoption of a single bus model and, therefore, the absence of any interaction among turbines (while aerodynamic mutual influence is modeled by 2% wind decrease), the overall production of the wind farm has been obtained from the results of five simulations, each of which has simulated the operation of one wind turbine for each row: in the aforementioned hypotheses, the power productions of wind turbines belonging to a specific row is the same.

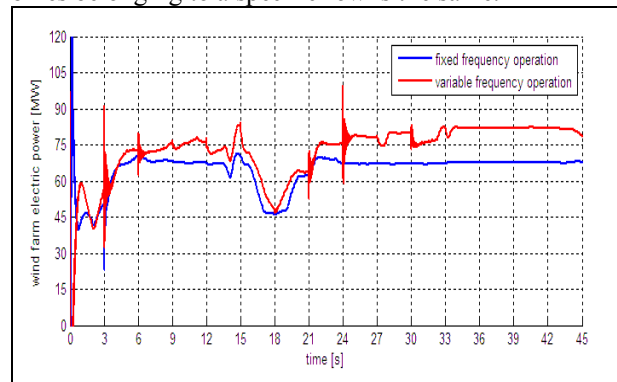


Figure 14: Comparison between the different operating mode

It is interesting pointing out that the power production in variable frequency operation results always higher than that one generated when the frequency is fixed, especially in high wind speed condition. This improvement was achieved without modifying the plant layout but only changing the operational strategy. Figure 14 shows that the power

increasing reaches 14 MW which correspond to about the 20 % of the wind farm production in fixed frequency operation. The power increase is mainly due to the DFIG power tracking curve widening caused by offshore frequency changing availability: this allows to reach higher rotational speeds (9) when DFIG converter is down-rated and then the generator slip is limited.

5 CONCLUSIONS

This paper developed of an appropriate control system for the synergic and real-time management of large offshore DFIG based wind farms, connected to the transmission network by VSC-HVDC link.

This plant layout allows variable frequency operation which let the DFIGs to improve their energy production. Set point signals have been calculated by means of a two-step online optimization procedure.

Test results have shown the model validation and the good response of the control system to variable frequency operation, highlighting the benefits of this operation mode, in terms of wind farm production when the generator slip is limited, and how the proposed tool is suitable for an optimized, coordinated and real time management of large offshore wind farms.

Future research will be focused on the development of a more realistic model, taking into account an appropriate VSC-HVDC modelling, the losses formulation, the inclusion of the AC offshore network topology and a more detailed characterization of the aerodynamic shading.

6 ACKNOWLEDGEMENTS

Francesco, Camillo, Mario, Pietro, Stefano and Ilaria gratefully thank Professor Paolo Marannino, teacher, colleague and friend deceased in May 2011, for his unforgettable kindness and teachings.

REFERENCES

- [1] GWEC (Global Wind Energy Council), "Global Wind Report 2009", March 2010
- [2] European Environment Agency (EEA), 2009: "Europe's onshore and offshore wind energy potential", Technical report No 6/2009
- [3] EWEA (European Wind Energy Association), "Pure Power – Wind energy targets for 2020 and 2030", December 2009
- [4] EWEA, "The European offshore wind industry – key trends and statistics 2009", January 2010
- [5] EWEA, "N. Fichaux, J. Wilkes, "Oceans of Opportunity: harnessing Europe's largest domestic energy resource" EWEA (European Wind Energy Association) Report 2009", September 2009
- [6] S. Muller, M. Deicke and R. W. De Doncker, "Doubly fed induction generator systems for wind turbine", IEEE Industry Applications Magazine, Vol.3, 2002
- [7] J. Arrilaga, Y. H. Liu, N. R. Watson, "Flexible Power Transmission, the HVDC Options", John Wiley & Sons, 2007
- [8] C. Feltes, I. Erlich, "Variable Frequency Operation of DFIG based Wind Farms connected to the Grid through VSC-HVDC Link", Power Engineering Society General Meeting, 2007, IEEE
- [9] Hau, E. Wind Turbines, Fundamentals, Technologies, Application, Economics, 2nd edition, 2006 Springer
- [10] T. Ackermann, "Wind Power in Power Systems", John Wiley & Sons, 2005
- [11] F. Careri, C. Genesi, P. Marannino, M. Montagna, S. Rossi, I. Siviero, "An online optimization algorithm for coordinated control of VSC-HVDC link and DFIGs for offshore wind applications", Innovative Smart Grid Technologies (ISGT) Europe, 2010, IEEE
- [12] I. Erlich, J. Kretschmann, J. Fortmann, S. Mueller-Engelhardt, H. Wrede, "Modeling of Wind Turbines Based on Doubly-Fed Induction Generators for Power System Stability Studies", IEEE Trans. on Power Systems, Vol. 22, No. 3, August 2007
- [13] A. Petersson, "Analysis, Modeling and Control of Doubly-Fed Induction Generators for Wind Turbines" Ph.D. Thesis, Division of Electrical Power Engineering, Department of Energy and Environment, Chalmers University of Technology, Goteborg, Sweden, 2005
- [14] C. Feltes, H. Wrede, F. W. Koch, I. Erlich "Enhanced Fault Ride-Through Method for Wind Farms Connected to the Grid Trough VSC-Based HVDC Transmission" IEEE Transactions on Power Systems Vol. 24, No. 3, August 2009
- [15] Nordex S77/1500 product data sheet, available on <http://www.nordex-online.com>
- [16] S. Li, T. A. Haskew, J. Jackson, "Integrated power characteristic study of DFIG and its frequency converter in wind power generation", Renewable energy 35 (2010), Elsevier